CFSRC COLLOQUIUM

Proceedings of the Cold-Formed Steel Research Consortium Colloquium
20-22 October 2020 (cfsrc.org)

Lateral Response of Cold-Formed Steel Framed Steel Sheathed In-line Wall Systems Detailed for Mid-Rise Buildings

A. Singh[1], X. Wang[2], Z. Zhang[3], F. Derveni[4], H. Castaneda[5], K.D. Peterman[6], B.W. Schafer[7], T.C. Hutchinson[8]

Abstract

Buildings constructed with cold formed steel (CFS) framing have shown great potential as a modern efficient building system. However, full understanding of their lateral structural behavior, particularly the contribution from non-designated systems, under seismic events is limited. The current North American Standards provide information that can be used to design CFS framed steel sheet shear walls which meet the seismic demands for low- to mid-rise (3-6 story) buildings. However, there is a paucity in experimental data to support design guidelines for taller mid-rise (>6 stories) and high-rise buildings (>10 stories), where large lateral load resistance is required. Moreover, existing code guidelines are based primarily on experiments involving shear walls subject to quasi-static monotonic and reversed cyclic loading protocols. In the current research project, shear walls placed in-line with gravity walls were tested at full-scale first under a sequence of increasing amplitude (in-plane) earthquake motions, and subsequently (for select specimens) under slow monotonic pull conditions to failure. Experiments were performed at the NHERI Large High-Performance Outdoor Shake Table at the University of California, San Diego. The selection of wall details was motivated by a CFS archetype building designed at 4 and 10 stories, as well as available experimental data. This paper documents the experimental response and physical damage observations of four wall specimen pairs in the test program. These particular specimens adopt compression chord stud packs with a steel tension tie-rods assembly, are either unfinished or finished on their exterior face, and laid out in a symmetric or asymmetric fashion. In addition, both Type I and “Type II” shear wall detailing are investigated.

1. Introduction

The construction industry in North America has seen substantial growth in the use of cold-formed steel (CFS) framed construction in recent years. The need for low cost, multi hazard resilient, mid-rise buildings has made CFS a popular choice as a construction material. CFS framing provides sustainable benefits for low- and mid-rise structures while also offering significant cost benefits. Some of the benefits of using CFS framing include lightweight framing, high durability and ductility, low installation costs particularly when prefabricated assemblies are used, and low maintenance costs due to its resistance to corrosion [1]. Additionally, steel offers a high strength to weight ratio while being a non-combustible material that resists fire spread in case of accidents. While this framing system has the potential to support the need for resilient housing, use of CFS has been restricted due to gaps in our understanding of their structural behavior in response to seismic events and by the limited guidelines provided in the design standards.

CFS walls commonly use Oriented Strand Boards (OSB), plywood or gypsum panels as sheathing on one or both sides of the wall. The behavior of CFS walls with these sheathing options have been investigated by several researchers [e.g. 2-7]. Adoption of steel sheet as a sheathing material in CFS shear walls is however relatively recent. As such, understanding of the structural behavior of steel sheet sheathed shear walls remains limited. Existing North American Standards, AISI S240 [8] & AISI S400 [9], are based on experiments involving shear walls subjected largely to quasi-static monotonic and reversed cyclic loading

[1] Graduate Student, Department of Structural Engineering, University of California, San Diego, La Jolla, CA, ams082@eng.ucsd.edu
[2] Postdoctoral Researcher, Department of Structural Engineering, University of California, San Diego, La Jolla, CA, xiw002@eng.ucsd.edu
[3] Graduate Student, Department of Civil and Systems Engineering, Johns Hopkins University, Baltimore, MD, zhidongzhang@jhu.edu
[4] Graduate Student, Department of Civil and Environmental Engineering, University of Massachusetts, Amherst, MA, fderveni@umass.edu
[5] Graduate Student, Department of Civil and Environmental Engineering, University of Massachusetts, Amherst, MA, hcastaneda@umass.edu
[6] Assistant Professor, Department of Civil and Environmental Engineering, University of Massachusetts, Amherst, MA, kdpeterman@umass.edu
[7] Professor, Department of Civil and Systems Engineering, Johns Hopkins University, Baltimore, MD, schafer@jhu.edu
[8] Professor, Department of Structural Engineering, University of California, San Diego, La Jolla, CA, tara@ucsd.edu

protocols such as [10-13]. Recent experimental efforts have tried to bridge the gap between the lateral capacities of cold-formed steel framed and hot-rolled steel shear walls [e.g. 14-16]. Shamim et. al. [17] was the first experimental effort aimed at dynamic characterization of steel sheathed CFS shear walls demonstrating consistent failure modes and seismic performance with existing literature However, an important limitation remains as prior testing programs have focused on isolated single shear wall specimens, with none integrating gravity walls within the specimen, though they are naturally configured along the same load resisting lines within buildings. Indeed, these wall components have to work together to support the architectural layout and building function. Moreover, gravity walls often have openings (doors and windows) and both exterior and interior walls have finishes installed for insulation purposes. As a result, understanding the structural behavior of CFS in-line walls, particularly the contribution from such *non-designated* lateral systems, under seismic events is limited. To this end, in the current research project, several of these limitations are addressed in an effort to enrich the experimental database with documentation regarding the performance of CFS framed wall assemblies.

2. Experimental Program

The CFS-NHERI in-line walls shake table experimental program involved testing of 8 wall configurations at the outdoor shake table at UC San Diego (nheri.ucsd.edu). Figure 2 shows an isometric and top view of the test setup. The large shake table footprint of 12.2 m × 7.6 m (40 ft × 25 ft) allowed for two pairs of nominally identical walls to be tested simultaneously. Earthquake input motions were applied in the east-west direction using the single axis shake table, which aligned with the long axis of the wall specimens. Two hollow steel sections served as top and bottom transfer beams which were connected to the specimens using two rows of 12.7 mm (0.5 in) A325 shear bolts. These transfer beams were post-tensioned to the shake table platen and the top concrete mass. The seismic weight for the wall pair consisted of a concrete slab (5.0 m × 3.0 m × 254 mm, 16.5 ft × 10 ft × 10 in), two steel plates (1.8 m × 3.0 m × 38 mm, 6 ft × 10 ft × 1.5 in) and the top transfer beams themselves, resulting in a total weight of 14.6 kN/m (1000 plf) per wall. Selection of the two configurations (four wall lines) to be tested simultaneously was based on their expected strength and initial stiffness. Similarity between the two wall pairs ensured that the scaled earthquake motions subjected them to the same target performance level.

Figure 3 shows the front view of the baseline wall specimen (SGGS-1) installed in the test setup and its framing details. For all the specimens in the test matrix, it is noted that the specimen names refers to the characteristics of a quadrant length of the specimen appended with the type of wall pair (either Type I or “Type II”), thus, the baseline specimen SGGS-1 is a Shear-Gravity-Gravity-Shear wall line with a Type I tie-rod (symmetric at shear wall ends) specimen. The dimensions of the individual walls were 4.88 m (16 ft) length and 2.74 m (9 ft) height. The baseline specimen was a symmetric, unfinished wall with a 2.44 m (8 ft) gravity wall segment in the middle and 1.22 m (4 ft) Type I shear wall segments on each end. Each shear wall segment was detailed with a pair of tie-down assemblies consisting of 600S250-97 toe-to-toe compression stud packs and a ϕ29 mm (ϕ1.125”) Grade B7 tension tie rod in the middle of the stud packs on each end of shear segment. The steel sheet used as sheathing was 0.76 mm (0.030”) thick with a nominal yield strength of 230 MPa (33 ksi). The sheathing was attached to the shear wall framing using No. 12 flat pan head screws at 51 mm (2”) o.c edge and 305 mm (12”) o.c field spacing. Shear segments were further strengthened by blocking at every third height of the wall. The gravity wall framing utilized 600S250-68 studs placed at 610 mm (2 ft) o.c. The top and bottom tracks were 600T250-97 members. Additionally, a 1200T250-97 ledger track was attached to the top of the wall on the rear face. All framing members had 345 MPa (50 ksi) nominal strength and were assembled using No. 10 flat pan head screws. These wall details were motivated from a designed CFS-framed archetype building which utilized the available experimental data and current code guidelines. A summary of the archetype building design can be found in [18].

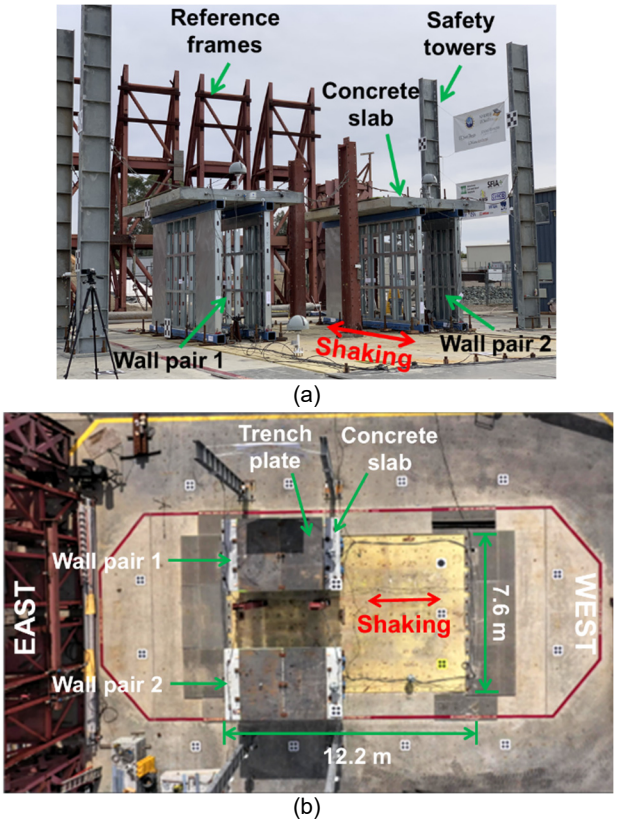

Figure 2: Shake table test setup: (a) Isometric view and (b) Top view

It should be noted that while eight wall pair configurations were tested, response of four select configurations is the subject of the present paper. These include:

1. SGGS-1: baseline wall specimen, which was constructed as a symmetric, unfinished wall with Type I shear wall detailing.
2. SGGS-1F: similar baseline framing with applied finish.
3. SGGS-2B: symmetric, unfinished wall with “Type II” shear wall detailing, with 305 mm o.c. fastener spacing along the interior edge of steel sheet.
4. SGGG-1: unsymmetrical, unfinished wall with a 4 ft shear wall segment with Type I detailing on only one wall end.

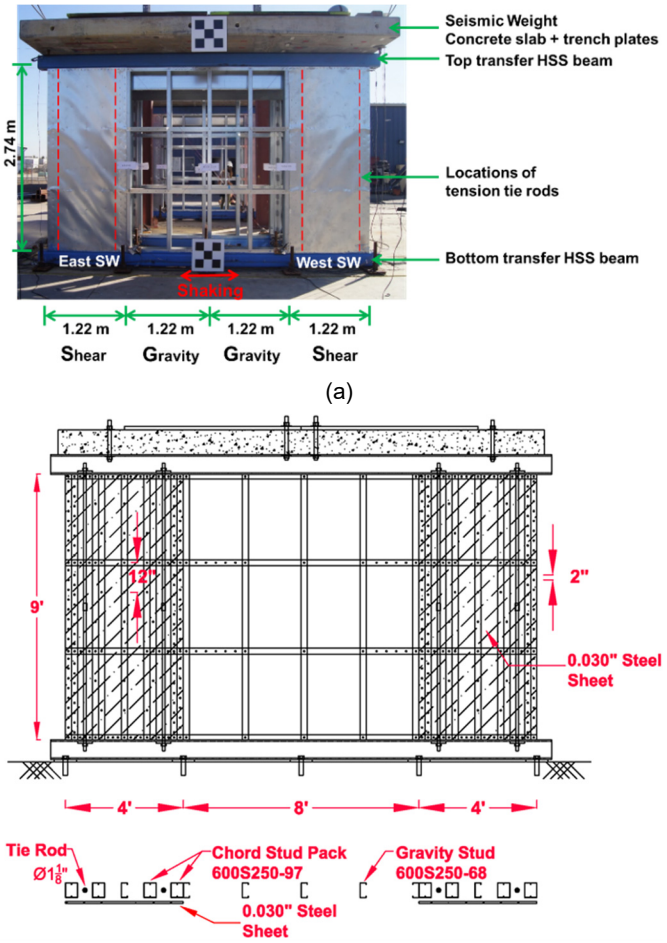

Figure 3: (a) Baseline specimen (SGGS-1) photograph as installed in test setup and (b) framing details

Figures 3 and 4 show the front view of the specimens. Walls with finish application had gypsum board on the interior face and glass-mat sheathing panels with Exterior Insulation Finish System (EIFS) on the exterior face installed in the field using No. 8 gauge 44 mm (1-3/4”) flat head screws at 152 mm (6”) o.c edge and 406 mm (16”) o.c field spacing. Installed gypsum boards were 1.22 m × 2.44 m × 16 mm (4 ft × 8 ft × 5/8 in) Firecode Type X, while glass-mat sheathing panels were 1.22 m × 2.74 m × 16 mm (4 ft × 9 ft × 5/8 in) Firecode Type X. Figure 5 shows the different steps involved in the EIFS application. It should be noted that specimen SGGS-2B was not designed and detailed with any members collecting and carrying the shear to the shear wall segments at the ends, this specimen is not a code compliant Type II shear wall as defined in AISI S400.

The two pairs of wall specimens concurrently on the table were densely instrumented with more than 120 analog sensors connected to a multi-node distributed data acquisition system that sampled data at a rate of 256 Hz. These analog sensors included: (a) accelerometers measuring top mass and shake table accelerations, (b) string potentiometers measuring top mass and table displacements as well as wall sheathing panel shear distortion, (c) strain gages measuring tension tie-rod strains, and (d) linear potentiometers measuring wall uplift.

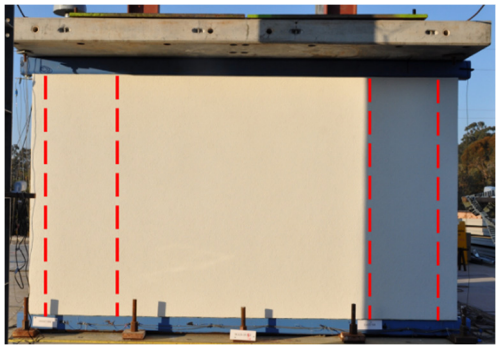

(a) SGGS-1F (finished with EIFS)

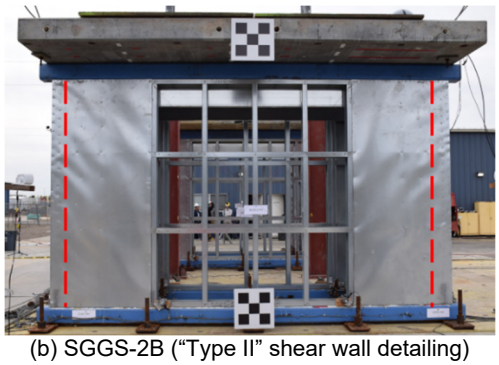

(b) SGGS-2B (“Type II” shear wall detailing)

(c) SGGG-1 (single shear wall unsymmetrical configuration)

Figure 4: Front view of the specimens
Note: Dashed lines show location of tension tie-rods

(a) Glass-mat sheathing installation

(b) 1" thick Expanded Polystyrene (EPS) foam boards attached using cement adhesive

(c) Rasping of foam boards before base coat application with embedded reinforcing mesh

(d) Second coat and finish coat application

Figure 5: Steps involved in EIFS application

The wall specimens were tested under a sequence of in-plane earthquake motions with increasing intensities, and subsequently, for select specimens, under slow monotonic pull conditions until a target 40% post-peak strength degradation, see Figure 6. Two test motions from two earthquake events, namely the: (a) 1994 M_w=6.7 Northridge earthquake (Canoga Park record component ID: CNP196) and (b) 2010 M_w=8.8 Maule earthquake in Chile (Curicó record component ID: CUR-EW) were selected as seed motions representative of strong earthquakes in California and long duration events with strong shaking [19]. Seed motion characteristics are shown in Figure 7. Additionally, low-amplitude white noise tests with root mean square (RMS) intensities of 1.5%g and 3%g and durations of 3 minutes were conducted before and after each earthquake test to determine the dynamic characteristics of the wall specimens at different damage states.

Based on a defined scaling procedure, earthquake motions with increasing intensities were selected for the specimens. Tables 1 through 3 summarize the peak ground acceleration (PGA) and peak ground displacement (PGD) of the achieved motions in the earthquake test sequence. The motion scaling strategy, which utilized pre-test numerical models and dynamic characteristics obtained from white-noise tests, provided reasonable scale factors for capturing the wall behavior at intended target performance levels: elastic, quasi-elastic, design, and above design. More details about the scaling procedure and performance level definitions can be found in [18]. Since the specimens SGGS-1 and SGGS-1F did not reach strength during the earthquake sequence, they were tested to failure through a slow monotonic pull test.

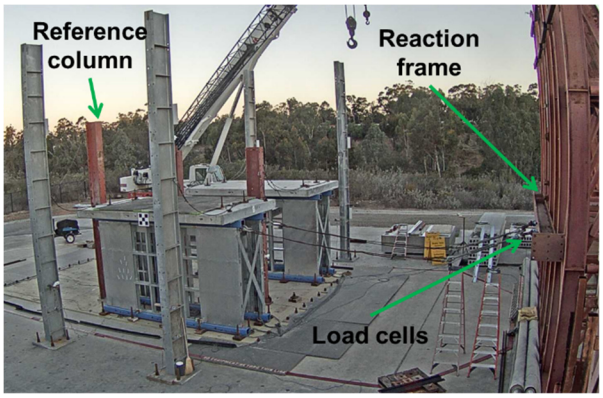

Figure 6: Monotonic pull test setup

Table 1: Earthquake test sequence: SGGS-1

Test Motion	Target Performance Level	PGA (*g*)	PGD (cm)
EQ1: CNP196	Elastic (E1)	0.31	7.69
EQ2: CUR-EW	Elastic (E2)	0.24	2.32
EQ3: CNP196	Quasi-elastic (QE)	0.66	17.66
EQ4: CNP196	Design event (DE)	1.20	35.0

Table 2: Earthquake test sequence: SGGS-1F

Test Motion	Target Performance Level	PGA (*g*)	PGD (cm)
EQ1: CNP196	Elastic (E1)	0.25	5.98
EQ2: CUR-EW	Elastic (E2)	0.15	1.41
EQ3: CNP196	Quasi-elastic (QE)	0.66	19.51
EQ4: CNP196	Design event (DE)	1.20	33.77
EQ5: CNP196	Above Design (ADE)	1.56	48.23

Table 3: Earthquake test sequence: SGGS-2 and SGGG-1

Test Motion	Target Performance Level	PGA (*g*)	PGD (cm)
EQ1: CNP196	Elastic (E1)	0.15	3.61
EQ2: CUR-EW	Elastic (E2)	0.11	1.16
EQ3: CNP196	Quasi-elastic (QE)	0.29	7.20
EQ4: CNP196	Design event (DE)	0.63	16.45
EQ5: CNP196	Above Design (ADE)	0.80	25.14

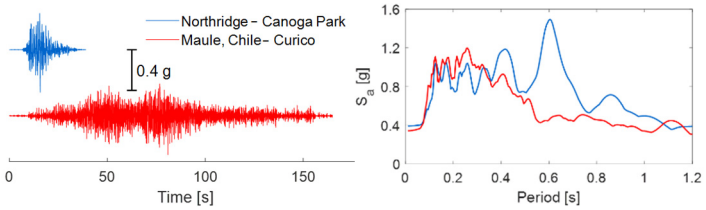

(a) (b)

Figure 7: Selected earthquake seed motions: (a) acceleration time histories and (b) pseudo-acceleration spectra (ξ = 5%)

3. Results and Discussion

3.1 Force-displacement behavior

Following the sequence of increasing amplitude earthquake motions as described above, and monotonic pull tests for select specimens, the force-displacement behavior of the specimens at different damage states could be derived. Figure 8 shows the force displacement behavior for the baseline specimen SGGS-1 during the earthquake tests and the subsequent monotonic pull test. Specimen response was essentially linear for the first three earthquake tests, with less than 0.4% achieved drift ratio and shear force below 50% strength. The specimen started showing non-linearity during the design event with 1% drift demand and 85% lateral strength. During the monotonic pull test, the specimen reached strength at 160.2 kN (36.0 kip) at a drift ratio of 1.95% and during continued pull demonstrated a post-peak degradation of 40% at 4.15% drift ratio. The elastic stiffness of the specimen, defined as the secant stiffness at 40% strength, was measured as 83.0 kN/cm (47.4 kip/in).

Figures 9 through 11 show the force-displacement behavior of the remaining specimens under consideration for the last earthquake test they were subjected to, and monotonic test, if applicable. In each case, the specimen response is compared to the hysteresis behavior of the baseline specimen SGGS-1. For specimen SGGS-1F, the specimen with finishes, the force-displacement response of the specimen was in the linear regime for the first three earthquake tests, with the achieved drift ratio less than 0.1% and the shear force remaining below 30% strength. This specimen behaved non-linearly during the tests EQ4 and EQ5 as the drift demand reached 0.9% and the shear force reached 60% of strength. During the monotonic pull test, the specimen reached strength at 208.2 kN (46.8 kip) at a drift ratio of 1.90%, and subsequently, a 40% post-peak degradation at 4.92% drift ratio. The elastic stiffness of the specimen, defined as the secant stiffness at 40% strength, was measured as 204.5 kN/cm (116.8 kip/in).

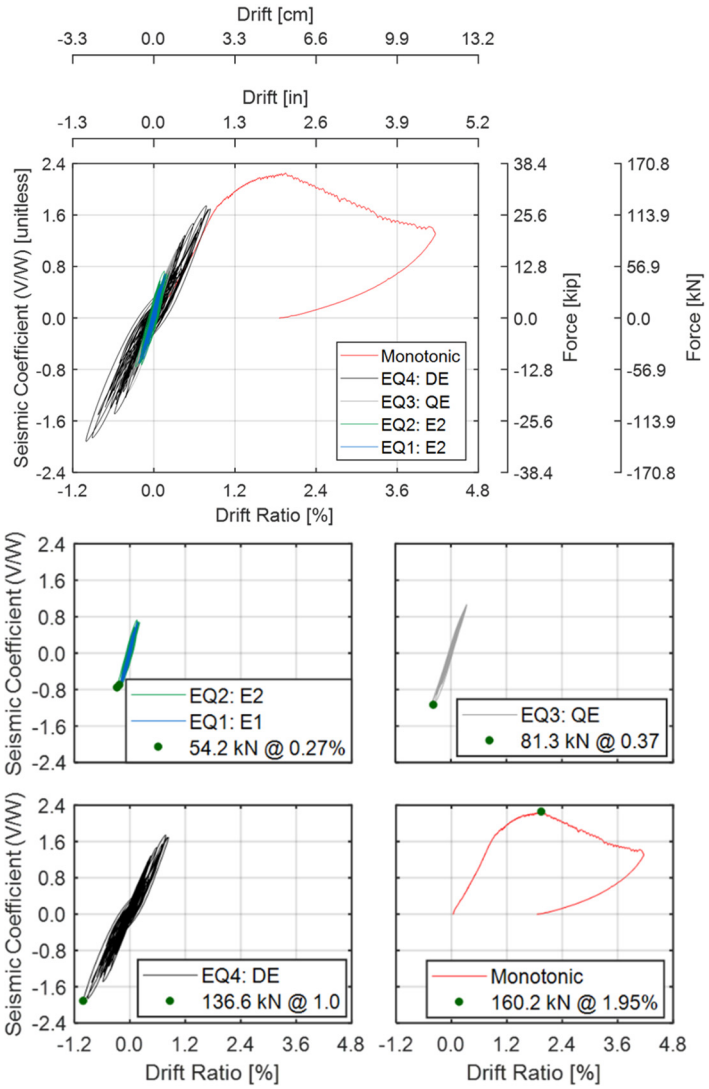

Figure 8: Force-displacement response of SGGS-1 specimen

The force-displacement response of specimen SGGS-2B ("Type II") remained essentially linear for the earthquake tests EQ1 to EQ3 with the achieved drift ratio less than 0.2% and shear force approaching 40% strength. The specimen showed non-linear behavior during EQ4 as drift demand reached 0.7% and shear demand approached strength. The specimen reached strength at 84.1 kN (18.9 kip) at a drift ratio of 1.22% during earthquake test EQ5 when it was pushed into the post-peak response as the drift demand exceeded 10%. The elastic stiffness of the specimen was measured as 70.7 kN/cm (40.4 kip/in).

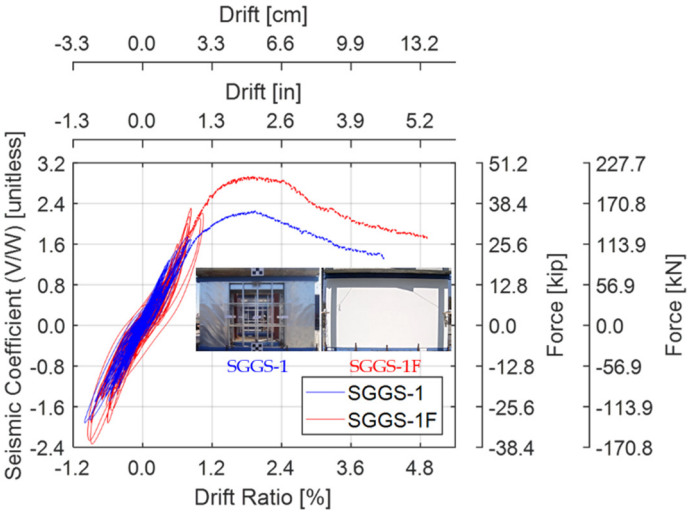

Figure 9: Force-displacement response of SGGS-1F specimen compared with SGGS-1 baseline specimen

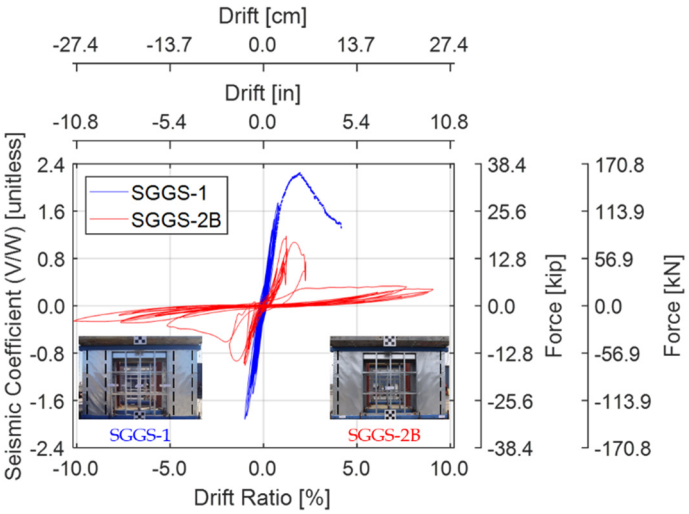

Figure 10: Force-displacement response of SGGS-2B specimen compared with SGGS-1 baseline specimen

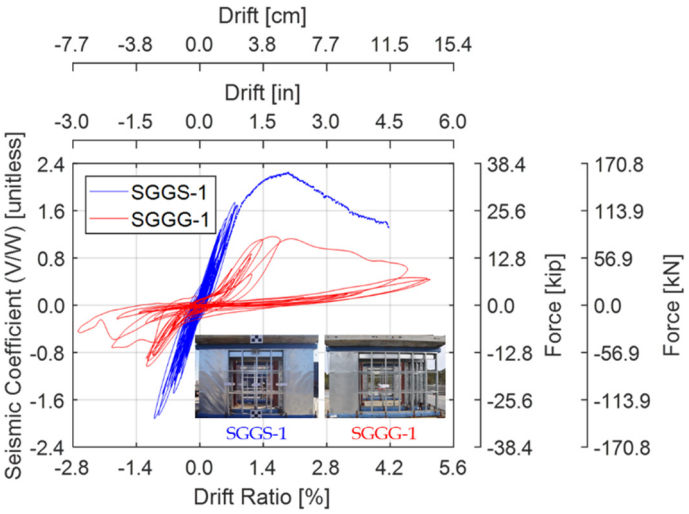

Figure 11: Force-displacement response of SGGG-1 specimen compared with SGGS-1 baseline specimen

Similarly, for specimen SGGG-1, an unsymmetrical wall configuration with a single shear wall, the force-displacement response of the specimen remained essentially linear for the earthquake tests EQ1 to EQ3 with the achieved drift ratio reaching 0.5% and the shear force approaching 55% of strength. The specimen showed non-linear behavior during EQ4 as the drift ratio demand reached 1.0% and shear demand reached 90% strength. The specimen reached strength at 82.7 kN (18.6 kip) at a drift ratio of 1.60% during earthquake test EQ5 when it was pushed into the post-peak region with drift demand exceeding 5%. The elastic stiffness of the specimen was measured as 39.1 kN/cm (22.3 kip/in).

Table 4: Summary of test results

Wall Configuration	Strength (kN)	Drift ratio at strength (%)	Elastic Stiffness (kN/cm)
SGGS-1	160.2	1.95	83.0
SGGS-1F	208.2	1.90	204.5
SGGS-2B	84.1	1.22	70.7
SGGG-1	82.7	1.60	39.1

3.2 Evolution of dynamic characteristics

The progression of damage in wall specimens manifest in the evolution of their natural period and damping ratio. Figures 12 and 13 show the evolution of these dynamic characteristics with lateral force normalized by individual specimen strength, identified at different damage stages using the 3%*g* RMS white noise tests conducted in between earthquake tests, for the four wall configurations under consideration. For the baseline specimen SGGS-1, the natural period elongated from 0.157s in its undamaged state to 0.199s after earthquake test EQ4. Finished specimen SGGS-1F was the stiffest with a natural period of 0.082s in its undamaged state. However, as damage accumulated in the specimen, in the form of the finish layer losing adherence to the framing, the natural period of the finished specimen approaches that of its unfinished baseline counterpart. As specimens SGGS-2B and SGGG-1 both used fewer tension rods and/or fewer shear wall segments, they were both significantly less stiff than the baseline specimen. Also, these specimens incurred more damage to their steel sheet and fasteners, as compared to specimen SGGS-1, before they reached strength. As a result, their natural period grew by a greater fraction of their undamaged natural period.

These components offered appreciable damping with each specimen offering between 2-3% damping (ζ_o) in their undamaged state. Amongst them, SGGS-1F had the highest damping ratio in its undamaged state at 3.3%. This can be attributed to the significantly greater number of fastener connections used to attach the gypsum and glass-mat panels. However, as specimens SGGS-2B and SGGG-1 incurred damage to their framing during the higher intensity earthquake tests, they demonstrated a larger

damping ratio. It should be noted that for specimen SGGS-1F, earthquake tests EQ4 and EQ5 had to be repeated due to top mass slip. Because the specimen had already incurred damage during those tests, the dynamic characteristics obtained after their repetitions show a sudden jump due to the accrued damage.

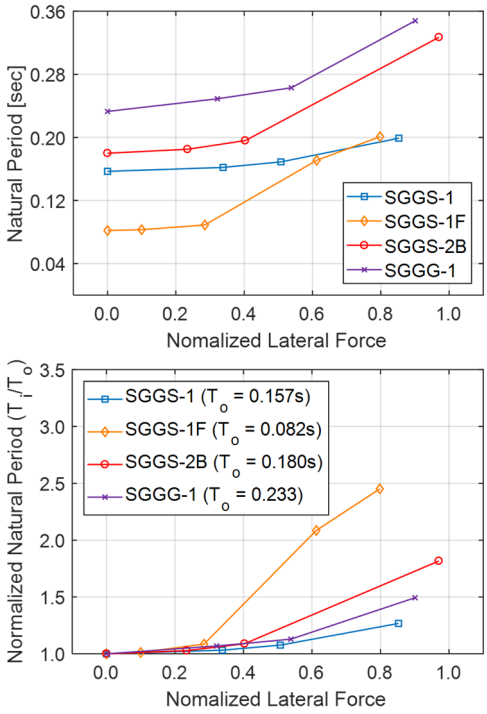

Figure 12: Evolution of natural period during earthquake tests

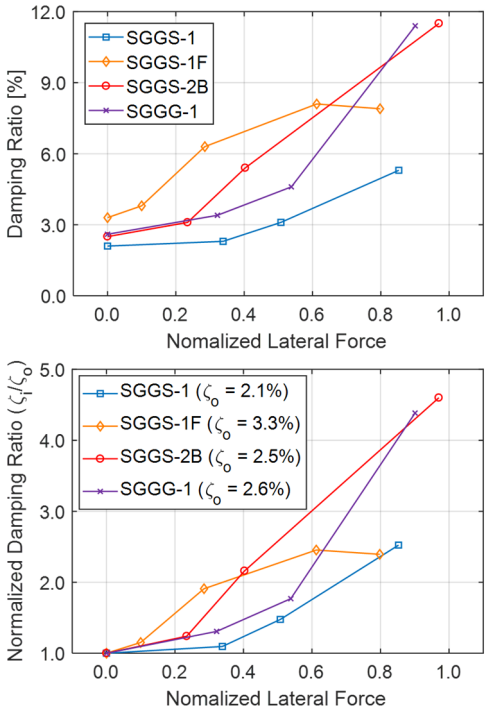

Figure 13: Evolution of damping ratio during earthquake tests

3.3 Physical damage observations

Non-linear behavior in specimen SGGS-1 initiated in earthquake test EQ4 along the shear wall tension field with buckling of the steel sheet widely distributed and readily observable lines of plastic deformation, remaining prominently visible at the end of the test. Fastener tilting and bearing onto the steel sheet was visible in ~20% of screws following this test, with most clustered at the corners of the steel sheet directly along the main diagonals of the tension field. Most of the damage occurred during the monotonic pull, when extensive shear buckling of the sheet was observed as the width of the tension field increased with drift demand, widening to include most of the steel sheathing. At the end of the monotonic pull test, local buckling of the gravity stud adjacent to the shear segment compression stud pack at diagonally opposite locations of the gravity wall segment was observed. However, the compression stud packs or track framing members did not experience any visible damage. By the end of the test, most screws showed some form of damage. Sheet pull over or edge tearing had spread from the corner to quarter height of the chord studs and a third length of top and bottom tracks and a few field screws in the middle of the sheet. Away from the main diagonal, fasteners along the off diagonals showed some tearing of sheet as screws tilted to large angles. Fasteners furthest away from the spread of tension field action showed bearing/tilting damage that they had suffered during earthquake tests primarily. Photographs documenting these physical damage observations are shown in Figure 14.

Specimen SGGS-1F also showed non-linearity during earthquake test EQ4 and EQ5, see Figure 15. Cracks in the EIFS layer could be seen along the height at the two ends of the walls with the embedded reinforcing mesh stretching across them. On the interior face, the gypsum panels experienced corner and boundary crushing against each other and ledger framing. One gypsum board became loose due to screw pull-through. Most of the damage occurred during the monotonic pull, as the EIFS layer along with the glass-mat sheathing panel substrate separated from the steel sheet underneath beginning from the two wall ends and propagating towards the gravity bay in the middle. The glass-mat sheathing had pulled over the fasteners connecting it to the CFS framing. EIFS layer could be seen to have warped out of plane. The gypsum panels on the inside suffered local crushing around the fasteners before becoming loose and detaching completely, pulling over the fasteners connecting it to the framing. A few framing screws for compression stud packs failed in head shear. As a result, the stud packs slipped along the bottom track. Bottom and top tracks were also damaged locally in the shear wall segments near the tension rod locations. Local buckling of the gravity stud adjacent to the shear segment compression stud pack at diagonally opposite locations of the gravity wall segment was observed, similar to SGGS-1 specimen. After

removing the EIFS layer, plastic deformation of the exposed steel sheet due to tension field action could be seen spread over the majority of sheet face. Sheet tearing and pull-over the fastener heads could be seen at the corners of the sheets and along the bottom edge.

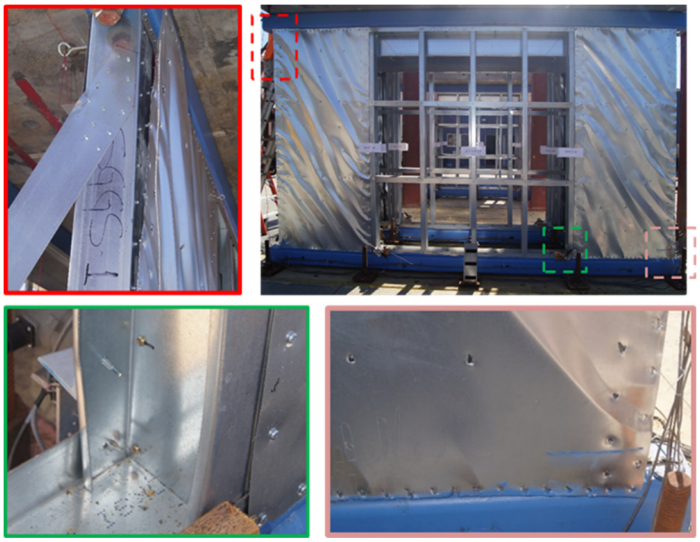

Figure 14: Photographs of SGGS-1 at end of monotonic test

Figure 15: Photographs of SGGS-1F at end of monotonic test

Specimen SGGS-2B showed non-linear behavior during EQ4 as the drift ratio demand reached 0.7%. At this point, all fasteners on the interior edge of the steel sheet were damaged extensively. Approximately 50% of the fasteners observed tearing along the steel sheet edge due to head tilt, while another 20% showed sheet pull over the screw head. Even at this intensity, plastic damage to the steel sheet was minimal. However, during earthquake test EQ5, the specimen was pushed into the post-peak region. Steel sheet pulled over the screw heads along the entire interior edge of sheet losing its entire ability to transfer any lateral load. Still, plastic damage to steel sheet remained minimal. Framing suffered extensive damage due to high drift demands. Chord stud pack and field stud framing connections suffered head shear failure. Local buckling of the gravity stud adjacent to the shear segment was observed. Bottom and top tracks also were locally damaged. Photographs documenting these physical damage observations are shown in Figure 16. However, it should be noted that even after being pushed to 10% drift, the system did not collapse and the residual drift after this earthquake test was insignificant, demonstrating the efficacy of the tension tie-rod system to prevent collapse.

Specimen SGGG-1 showed non-linear behavior during EQ4 as the drift ratio demand reached 1.0%. However, all damage was confined to the widening of the tension field and distributed buckling of the steel sheet. Fastener tilting and bearing onto the steel sheet was visible in ~20% of screws, with most being edge screws clustered at corners of sheet along the main diagonals of the tension field. However, during earthquake test EQ5, the specimen was pushed into the post-peak region as the drift demand exceeded 5%. Extensive shear buckling of the sheet was observed during the earthquake test as width of tension field grew to cover the entire steel sheet. At the end of the test, steel sheet had pulled over ~40% of the fastener heads. Others also showed tearing or bearing due to tilting at large angle. Framing suffered extensive damage due to high drift demands. Chord stud pack and field studs framing connections failed in head shear. Due to framing connection failure, chord stud packs slipped along bottom track. Gravity stud adjacent to the shear segment showed local buckling. Photographs documenting these physical damage observations are shown in Figure 17.

Figure 16: SGGS-2B specimen damage photographs after earthquake test EQ5

Figure 17: SGGG-1 specimen damage photographs after earthquake test EQ5

4. Conclusions

As part of the CFS-NHERI in-line walls shake table experimental program, eight pairs of wall configurations, shear walls placed in-line with gravity walls, were tested at full-scale under a sequence of increasing amplitude earthquake motions at the NHERI Large High-Performance Outdoor Shake Table at the University of California, San Diego. Characterizing the dynamic performance of long CFS framed walls subjected to earthquake motions was one of the main objectives of the experimental effort. The response of four of these configurations is summarized in the present paper, notably allowing comparison of exterior finish, “Type II” detailing, and unsymmetrical shear wall layout. In the presence of finish, an approximate 30% or 9.85 kN/m (675 plf) strength gain was observed without any significant change in the drift at which strength is achieved. Initial stiffness also increased by 150% due to finish application. However, as the finish layer started to lose adherence to the underneath framing, the natural period of the finished specimen approached that of its unfinished baseline counterpart. Due to the reduced number of tension rods and steel sheet fasteners, the “Type II” specimen had a lower strength when compared to the Type I baseline specimen. Additionally, the drift at which strength was achieved was also significantly lower for this specimen. Initial stiffness decreased by 50% for this specimen. Finally, the “Type II” specimen incurred more extensive damage to its steel sheet and fasteners, as compared to the baseline Type I specimen, before they reached strength. As a result, the “Type II” specimen became considerably less stiff with damage propagation. Similarly, the unsymmetrical specimen had 48% lower strength as compared to the symmetrical baseline specimen. Its elastic stiffness also decreased by 53% as a direct consequence of the reduced number of shear wall segments. It was expected that gravity wall segment would contribute to wall lateral strength. However, a 50% decrease in shear wall segments led to a 50% decrease in lateral strength. The evolution of the dynamic characteristics for the unsymmetrical specimen SGGG-1 was similar to that of the “Type II” specimen SGGS-2B.

5. Acknowledgments

The research presented is funded through the National Science Foundation (NSF) grants CMMI 1663569 and CMMI 1663348, project entitled: Collaborative Research: Seismic Resiliency of Repetitively Framed Mid-Rise Cold-Formed Steel Buildings. Ongoing research is a result of collaboration between three academic institutions: University of California, San Diego, Johns Hopkins University and University of Massachusetts Amherst, two institutional granting agencies: American Iron and Steel Institute and Steel Framing Industry Association and ten industry partners. Industry sponsors include ClarkDietrich Building Systems, California Expanded Metal Products Co. (CEMCO), SWS Panel and several others who each provided financial, construction, and materials support. Regarding support for the test program, the efforts of NHERI@UCSD staff, namely, Robert Beckley, Darren McKay, Jeremy Fitcher, and Alex Sherman, and graduate student Filippo Sirotti are greatly appreciated. Findings, opinions, and conclusions are those of the authors and do not necessarily reflect those of the sponsoring organizations.

References

[1] Schafer, B. W. (2011). Cold-formed steel structures around the world: A review of recent advances in applications, analysis and design. *Steel Construction*, *4*(3), 141-149.

[2] Serrette, R., Nyugen, H., Hall, G. (1996) Shear Wall Values for Light Weight Steel Framing', Report No. LGSRG-3-96, Department of Civil Engineering, Santa Clara University, Santa Clara, California, USA.

[3] Serrette, R. L., Encalada, J., Juadines, M., & Nguyen, H. (1997). Static racking behavior of plywood, OSB, gypsum, and fiberbond walls with metal framing. *Journal of Structural Engineering*, *123*(8), 1079-1086.

[4] Chen, C.Y. (2004) 'Testing and performance of steel frame / wood panel shear walls', Master Thesis, Advisor: Colin A. Rogers, McGill University, Montreal, Canada, August.

[5] Hikita, K. (2006) 'Combined gravity and lateral loading of light gauge steel frame / wood panel shear walls', Master Thesis, Advisor: Colin A. Rogers, McGill University, Montreal, Canada, December.

[6] Liu, P.; Peterman, K. D.; Yu, C.; and Schafer, B. W., "Characterization of Cold-formed Steel Shear Wall Behavior under Cyclic Loading for the CFS-NEES

Building" (2012). *International Specialty Conference on Cold-Formed Steel Structures*. 5.

[7] Lu, S. (2015) 'Influence of gypsum panels on the response of cold-formed steel framed shear walls', Master Thesis, Advisor: Colin A. Rogers, McGill University, Montreal, Canada, May.

[8] AISI S240 (2015) North American Standard for Cold-Formed Steel Structural Framing. American Iron and Steel Institute. AISI S240-15.

[9] AISI S400 (2015) North American Standard for Seismic Design of Cold-Formed Steel Structural Systems. American Iron and Steel Institute. AISI S400-15.

[10] Serrette, R., Enchalada, J., Hall, G., Matchen, B., Nyugen, H., Williams, A. (1997) 'Additional shear wall values for light weight steel framing', Report No. LGSRG-I-97, Department of Civil Engineering, Santa Clara University, Santa Clara, California, USA.

[11] Yu, C., Vora, H., Dainard, T., Tucker, J., Veetvkuri, P. (2007) 'Steel sheated options for cold-formed steel framed shear walls assemblies providing shear resistance', Report No. UNT-G76234, Department of Engineering Technology, University of North Texas, Denton, Texas, USA.

[12] Yu, C. (2010). Shear resistance of cold-formed steel framed shear walls with 0.686 mm, 0.762 mm, and 0.838 mm steel sheet sheathing. *Engineering Structures*, *32*(6), 1522-1529.

[13] DaBreo J, Balh N, Ong-Tone C, Rogers C.A. (2014) “Steel sheathed - cold-formed steel framed shear walls subjected to lateral and gravity loading.” *Thin-Walled Structures*, *74*, 232-245

[14] Rizk, R., Rogers, C.A. (2017) “Higher capacity cold-formed steel framed/steel shear walls for midrise construction.” Res. Report, Dept. of Civ. Eng. and Applied Mech., McGill University.

[15] Santos, V., Rogers, C.A. (2017) “Higher capacity cold-formed steel sheathed and framed shear walls for mid-rise buildings: Part 1.” Res. Report, Dept. of Civ. Eng. and Applied Mech., McGill University.

[16] Briere, V., Rogers, C.A. (2017) “Higher capacity cold-formed steel sheathed and framed shear walls for mid-rise buildings: Part 2.” Res. Report, Dept. of Civ. Eng. and Applied Mech., McGill University.

[17] Shamim, I., DaBreo, J., and Rogers, C. A. (2013). “Dynamic testing of single-and double-story steel-sheathed cold-formed steel-framed shear walls.” *Journal of Structural Engineering, 139*(5), 807-817.

[18] Singh, A., Wang, X., Torabian, S., Hutchinson, T. C., Peterman, K. D., & Schafer, B. W. (2020, April). Seismic Performance of Symmetric Unfinished CFS In-Line Wall Systems. In *Structures Congress 2020* (pp. 629-642). Reston, VA: American Society of Civil Engineers.

[19] Hutchinson, T.C., Wang, X., Hegemier, G., Meacham, B., Kamath, P., Sesma, F., and Holcomb, K. (2017). “Earthquake and Post-Earthquake Fire Performance of a Mid-Rise Cold-Formed Steel Framed Building.” *Proc., 2017 SEAOC Convention*, San Diego, CA.